Applied Catalysis B: Environmental 91 (2009) 1–10

Contents lists available at ScienceDirect

Applied Catalysis B: Environmental

journal homepage: www.elsevier.com/locate/apcatb

Review

Progress in development of direct dimethyl ether fuel cells

Alexey Serov *, Chan Kwak

Corporate R&D Center, Samsung SDI, Shin-dong 575, Yeongtong-gu, Suwon-si, Gyeonggi-do 443-731, South Korea

ARTICLE INFO

Article history:
Received 30 March 2009
Received in revised form 16 June 2009
Accepted 18 June 2009
Available online 25 June 2009

Keywords:
Dimethyl ether
Fuel cell
Anode
Catalyst

ABSTRACT

The present review summarizes recent research achievements related to the use of alternative fuel (specifically, dimethyl ether) in portable fuel cell devices. This review discusses the development of new electrocatalysts for successful dimethyl ether (DME) oxidation, the preparation and performance of membrane electrode assemblies (MEAs) and the effects of different fuel cell operation conditions The mechanisms of processes occurring at the anode and cathode are described, as shown in the literature. Different MEA structures are suggested for the purpose of altering the catalytic activity of anode catalysts and thereby improving the power output of direct DME fuel cells.

Contents

1. Introduction

Recently, the rapid development of powerful portable devices, such as notebooks, mobile phones, personal media players (PMPs), and personal digital assistants (PDAs) significantly increased the demand for high power output from batteries. Despite intensive research and development, lithium ion and metal hydride batteries cannot increase energy output without increasing the total weight of the device. These batteries should be replaced by new alternative power suppliers in the near future. Fuel cells that are operated by the direct feeding principle at elevated temperature and pressure can be used as substitutes for conventional batteries in portable applications. Several classes of fuel cells use liquid fuels, namely, methanol (direct methanol fuel cells) [1–11], ethanol (direct ethanol fuel cells) [12–22], formic acid (direct formic acid fuel cells) [23–30], and dimethyl ether (direct DME fuel cells) [31–44], amongst others. These fuel cells were the subject of investigation by both academic researchers and commercial R&D centers. Amongst these fuel cells, DMFC technology is the most developed and is nearly ready for commercialization. Nevertheless, using methanol as a fuel for DMFCs has several drawbacks, and these are preventing DMFCs from successful mass production. Methanol's toxicity is one such drawback; CH_3OH has a well-known poisonous effect upon skin contact and inhalation. The problem with using methanol as a fuel for DMFCs, at least from the environmental viewpoint, is that methanol easily spreads into ground water. The disadvantages associated with other liquid fuels are usually low performance (i.e., ethanol) or high corrosion (i.e., formic acid).

As shown previously, DME is practically free of drawbacks associated with other liquid fuels, and even has some significant advantages [35]. The main advantages can be summarized as follows:

* Corresponding author. Present address: Paul Scherrer Institute, 5232 Villigen PSI, Switzerland. Tel.: +41 56 5345251; fax: +41 56 3104435.
E-mail addresses: alexey.serov@psi.ch (A. Serov), kcpmhkj@yahoo.com (C. Kwak).

0926-3373/$ – see front matter © 2009 Elsevier B.V. All rights reserved.
doi:10.1016/j.apcatb.2009.06.018

- DME has reduced theoretical fuel requirements due to the high electron transfer number of 12, which is needed for complete oxidation to CO_2 (in comparison methanol, which has 6 electrons and only 2 hydrogens);
- DME is the simplest ether with no C–C bonds, which makes complete oxidation possible with a minimum kinetic energy loss [45];
- the dipole moment of DME is smaller than that of methanol, which leads to decreases in DME crossover from the anode to the cathode side;
- DME can be easily stored at high pressure like LPG and transferred from a tank to the fuel cell system without an additional pump;
- DME itself possesses low toxicity, does not spread into ground water;
- DME is less explosive than methanol and hydrogen.

Although DME is less active than methanol during oxidation on conventional catalysts and at normal fuel cell operation conditions (T = 50 °C and p = 1 bar) [46], the performance of direct DME fuel cells (DDMEFCs) at p = 5 bar and T = 130 °C was almost the same as the DMFC when the DMFC operated at normal fuel cell operating conditions [45]. Thus, dimethyl ether is a promising fuel for direct-feed fuel cells.

In the last 10 years, several groups of researches around the world investigated mechanisms of DME oxidation to find and develop new electrocatalysts. Attempts were made to increase DDMEFC performance by improving MEA performance, and by varying fuel composition and operation conditions. The present review describes recent achievements made in the field of DDMEFCs.

2. Mechanism of DME oxidation

Analysis of the by-products from anode exhaust suggests several possible mechanisms for DME oxidation. Trace amounts of methanol in the by-products of dimethyl ether oxidation were detected by Müller et al. [45]. Based on this data, they proposed that one methyl group was oxidized and hydrolyzed to form MeOH by cleaving the C–O–C bond. A different mechanism was suggested by Tsutsumi et al. [47]. During their investigation, under atmospheric pressure and T = 80 °C, formic acid was detected on the anode side. The amount of formic acid increased with increases in current density, and the authors detected neither methanol nor formaldehyde. This experimental observation suggested that both methyl groups were oxidized simultaneously and that two COHs were formed due to the cleavage of the C–O–C bond. Information about mechanisms taking place during DME oxidation is important for the design of new, more efficient catalysts for DDMEFCs.

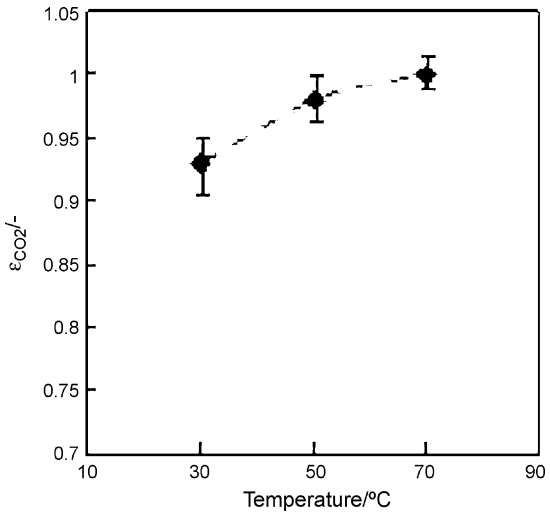

Fig. 1. Dependence of CO_2 current efficiency of DME on temperature at Pt/C in a half-cell at 600 mV in 1 M H_2SO_4. Reprinted from [31] with permission from Elsevier.

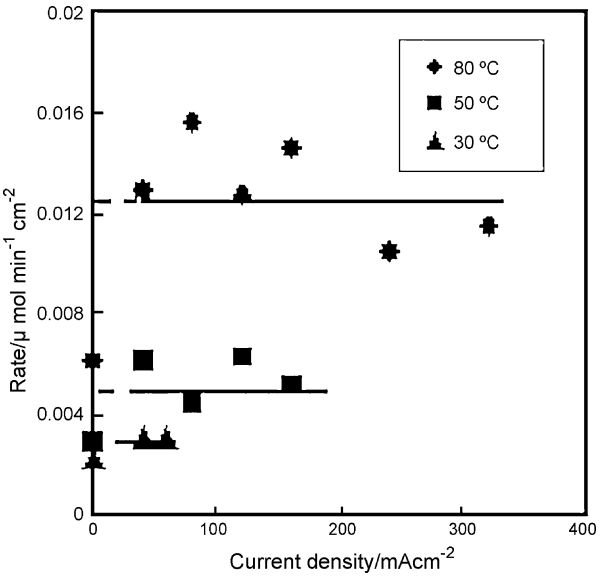

Fig. 2. Dependence of the rate of methanol formation in DDMEFC on current density determined by the anode exhaust. Reprinted from [31] with permission from Elsevier.

Recently, several studies investigated the processes occurring at the anode side during the operation of the DME fuel cells [31,36–38]. Mizutani et al. reported data on DME oxidation on Pt/C catalysts [31]. They found that in half-cell experiments, CO_2 current efficiency increased with increases in temperature (Fig. 1), reaching almost 1 at T = 70 °C. The tendency for CO_2 current efficiency to increase with increasing temperature in case of DME oxidation also holds true for methanol electrooxidation [48]. Comparison of these values shows that the current efficiency of DME is higher than that of methanol [49]. The authors also investigated the reaction products from the anode side of the MEA

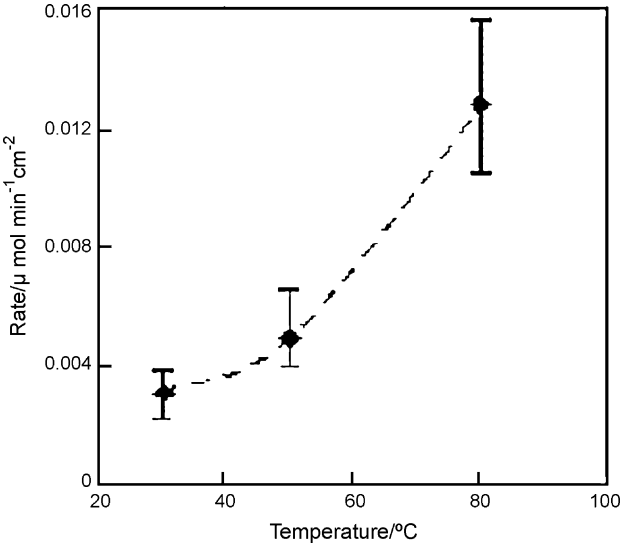

Fig. 3. Dependence of the rate of methanol formation in DDMEFC on temperature determined by the anode exhaust. Reprinted from [31] with permission from Elsevier.

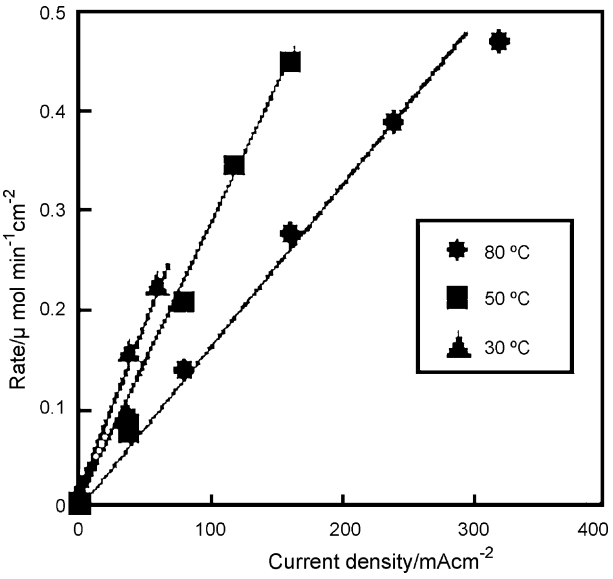

Fig. 4. Dependence of the rate of methyl formate formation in DDMEFC on current density determined by the anode exhaust. Reprinted from [31] with permission from Elsevier.

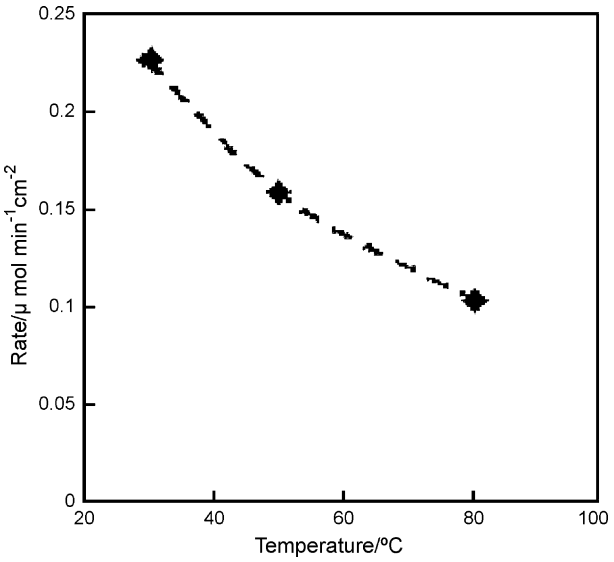

Fig. 5. Dependence of the rate of methyl formate formation in DDMEFC at 60 mA cm^{-2} on temperature determined by the anode exhaust. Reprinted from [31] with permission from Elsevier.

operated under DDMEFC conditions. They found that DME is mostly oxidized to CO_2 at high temperature; such data are in good correlation with results obtained in half-cell experiments. The main by-products of DME oxidation in DDMEFC were methanol and methyl formate. The rate of methanol production as a function of current density and temperature is shown in Figs. 2 and 3, respectively. As seen in the figures, the methanol production rate does not depend on current density but increases with increasing temperature. Based on this, methanol is probably not produced in an electrochemical reaction. One possible production mechanism is the hydrolysis of DME (Eq. (1)):

$$CH_3OCH_3 + H_2O \rightarrow 2CH_3OH \quad (1)$$

Figs. 4 and 5 show the production rate of methyl formate as a function of current density and temperature, respectively. A proportional increase in the methyl formate production rate with increases in current density reflect the electrochemical nature of this reaction. The methyl formate is probably produced by the following process (Eq. (2)):

$$CH_3OCH_3 + H_2O \rightarrow HCOOCH_3 + 4H^+ + 4e^- \quad (2)$$

From the temperature dependence of methyl formate production (Fig. 5), the authors concluded that CO_2 production is a preferable process at higher temperature as compared to $HCOOCH_3$ production.

During investigation of electrooxidation of DME on bulk platinum electrode Kerangueven et al. showed that the DME adsorption was a slow step in the overall oxidation reaction [32]. It was also found that DME adsorption is potentially dependent on the hydrogen region of platinum and independent of the double layer region. From low potential scan rate voltammetry and DME stripping experiments, it was shown that the DME oxidation occurred via several reaction paths. In situ IR reflectance spectroscopy detected linearly bonded CO (CO_L), bridge-bonded CO (CO_B), adsorbed COOH species and CO_2. From these electrochemical and spectro-electrochemical results, it was proposed that some adsorbed DME was hydrolyzed or directly oxidized to CO_2 or HCOOH species remaining Pt–CHO and/or Pt–CO surface species on the platinum sites. As a result of this detailed study the authors suggested the following mechanism of DME oxidation. The adsorption of DME blocks a part of the platinum surface at low potentials leaving the other part of the platinum surface free for direct DME oxidation. In this mechanism, one has to take into account the formation of methanol, formic acid and CO_2 at low potentials in addition to the formation of linearly and bridge-bonded CO species. In the low potential range, the direct oxidation of DME can occur via C-adsorption and hydrolysis of the molecule

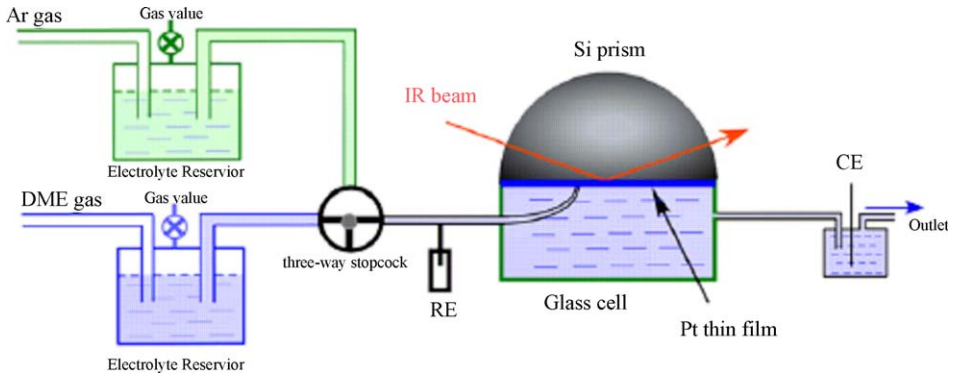

Fig. 6. A simplified scheme for the flow IR cell used in [37]. Reprinted from [37] with permission from Elsevier.

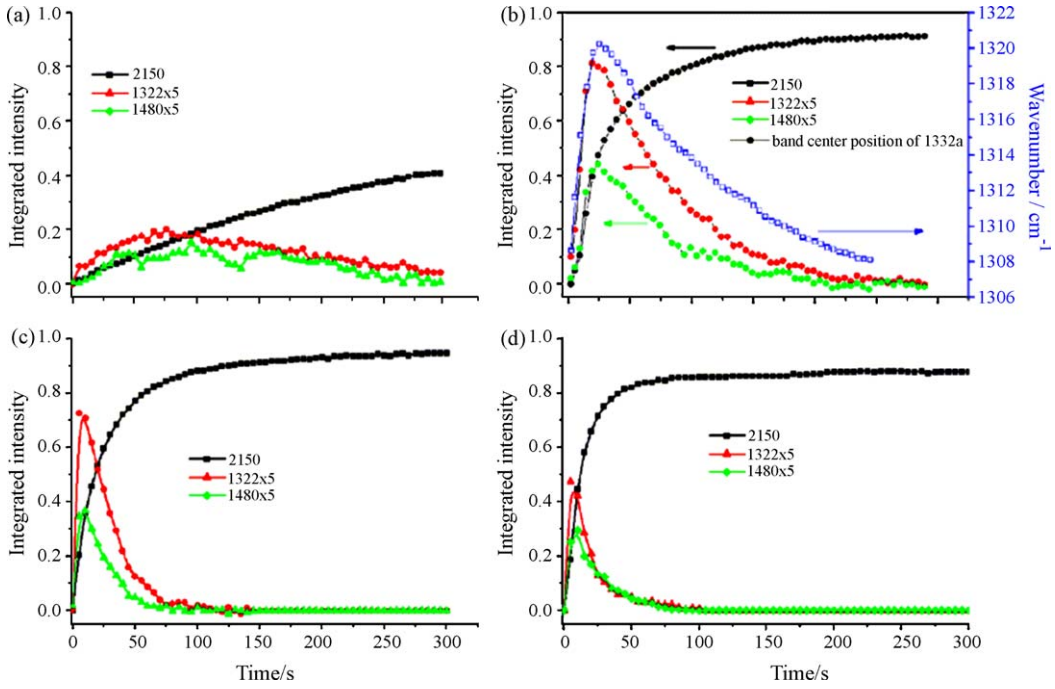

Fig. 7. The integrated band intensities taken from a series of in situ IR spectra simultaneously acquired in the potential step from 0.05 V to (a) 0.1 V, (b) 0.2 V, (c) 0.4 V and (d) 0.5 V; the band center of 1322 cm^{-1} at 0.2 V (hollow). The intensities of bands at 1322 and 1480 cm^{-1} are multiplied by five times. Reprinted from [37] with permission from Elsevier.

giving a current plateau:

$$CH_3{-}O{-}CH_3 + H_2O \rightarrow CH_2OH_{ad} + CH_3OH + H^+ + e^- \quad (3)$$

and/or

$$CH_3{-}O{-}CH_3 + H_2O \rightarrow CH_2OH_{ad} + 2H^+ + 2e^- \quad (4)$$

followed by:

$$CH_2OH_{ad} \rightarrow CHO_{ad} + 2H^+ + 2e^- \quad (5)$$

then,

$$CHO_{ad} + H_2O \rightarrow CO_2 + 3H^+ + 3e^- \quad (6)$$

and/or

$$CHO_{ad} + H_2O \rightarrow HCOOH + H^+ + e^- \quad (7)$$

and/or

$$CHO_{ad} \rightarrow CO_{ad} + H^+ + e^- \quad (8)$$

At higher potentials (higher than 0.55 V vs. RHE), platinum is able to activate water and can adsorb OH species:

$$CHO_{ad} + OH_{ad} \rightarrow CO_2 + 2H^+ + 2e^- \quad (9)$$

and,

$$CO_{ad} + OH_{ad} \rightarrow CO_2 + H^+ + e^- \quad (10)$$

The authors concluded that more detailed in situ IR spectroscopic measurements and analysis of the distribution of reaction products as a function of the electrode potential were necessary in order to determine the reaction products as well as the adsorbed intermediates.

Later, a study of dimethyl ether oxidation on a platinum surface with a focus on determining the intermediate adsorption species and oxidation pathways of DME was performed by Liu et al. [36]. Using both electrochemical measurements and in situ attenuated total reflection-Fourier transform infrared spectroscopy (ATR-FTIR), they showed that the coverage of the adsorption species (θ_{ads}) was ca. 90% for the DME oxidation reaction at $0.1 < E < 0.45$ V on the Pt. Also, the main intermediate adsorption species (besides CO) on the surface of the catalyst were–COOH, –CHO, –HCOO– and –OCH_3. They concluded their research with the recommendation that new electrocatalysts be developed, specifically electrocatalysts stable enough to avoid the poisonous the effect of CO. Such new catalysts could be based on platinum alloys with transition metals, such as PtRu, PtSn, etc.

Zhang et al. [37] attempted to determine the mechanism of DME oxidation by using electrochemical and in situ infrared (IR)

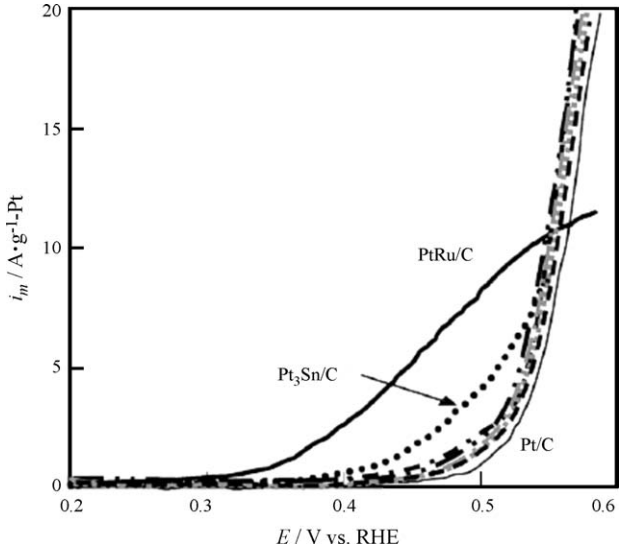

Fig. 8. Mass activities for the DME oxidation reaction (DOR on PtMe/C and Pt/C measured by slow scan voltammetry in 1 M H_2SO_4 at 50 °C. Scan rate: 1 mV s^{-1} (▬▬) PtRu/C, (• • •) Pt_3Sn/C, (▬ ▮ ▬) Pt_3Mo/C, (. . . . .) PtW/C, (▬▬ ▬) PtCo/C, (- ·· - ··) Pt_2Cr/C, (▬ ▪ ▬) PtNi/C and (▬) Pt/C. Reprinted from [39] with permission from Elsevier.

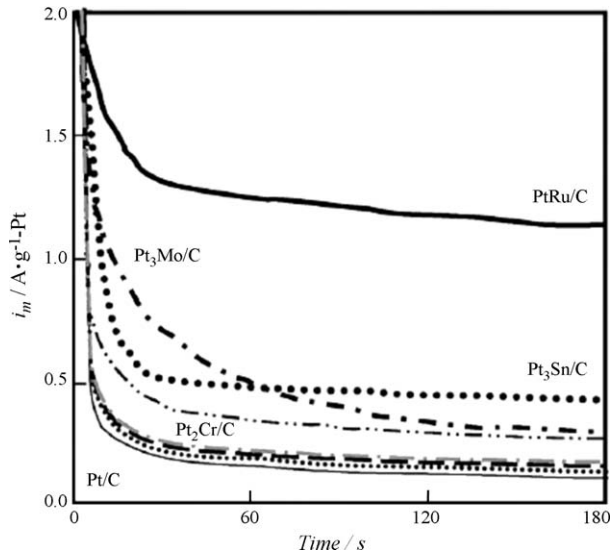

Fig. 9. Current–time curves measured at 0.4 V on PtMe/Cs and R/C in DME saturated 1 M H_2SO_4 at 50 °C. (▬▬) PtRu/C, (• • •) Pt_3Sn/C, (▬ ▪ ▬) Pt_3Mo/C, (. . . . .) PtW/C, (▬▬ ▬) PtCo/C, (▪ ·· ▪ ··) Pt_2Cr/C, (▬ ▪ ▬) PtNi/C and (▬) Pt/C. Reprinted from [39] with permission from Elsevier.

measurements. To avoid the influence of diffusion and accumulation problems from soluble species, a spectroscopic flow-cell with Kretschmann ATR configuration was newly designed and employed in the in situ IR measurement (Fig. 6). A supply of reactant at a constant concentration and the quick removal of soluble products in the solution side allows for the investigation of species on the electrode surface. Using this in situ IR measurement, the transient processes of DME decomposition at different potentials could be clearly observed. A summary of the results of the in situ IR measurements are presented in Fig. 7. At 0.1 V, bands related to $(CH_3OCH_2-)_{ad}$ are still weak; linearly bonded carbon monoxide grows slowly with time but no saturation coverage is reached. When the potential is higher than 0.2 V, the formation rate of $(CH_3OCH_2-)_{ad}$ and CO_L increases quickly. $(CH_3OCH_2-)_{ad}$ reaches maximum intensity and then decreases to zero while CO_L increases monotonously in the beginning and

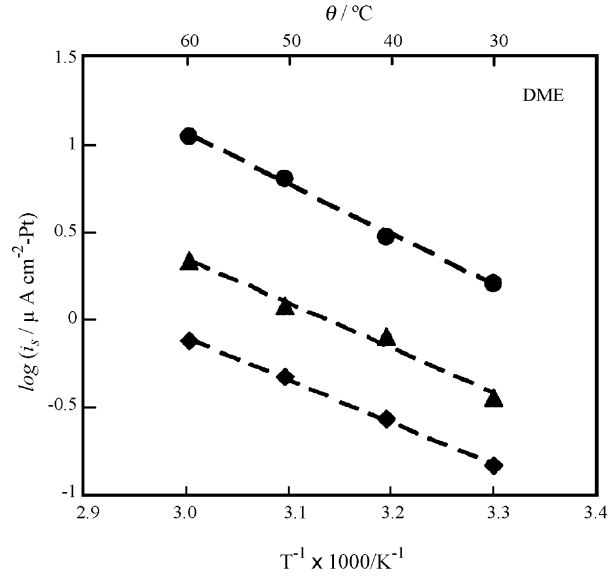

Fig. 10. Arrhenius plots for DME oxidation current densities obtained after 600 s at 0.4 V on PtRu/C: (●) Pt_3Sn/C, (▲), Pt/C and (◆) in 1 M H_2SO_4. Reprinted from [39] with permission from Elsevier.

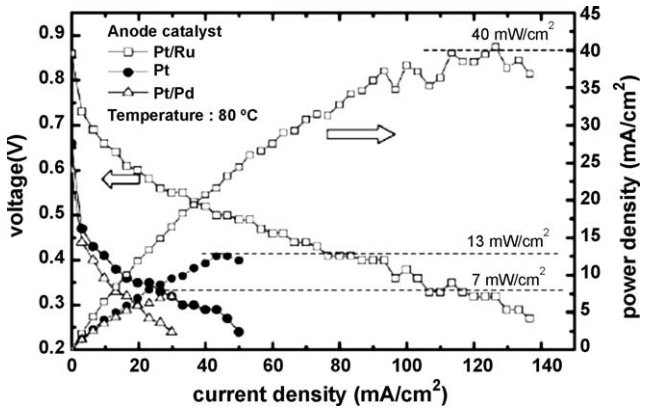

Fig. 11. Effect of anode catalysts on the performance of the fuel cell using the DME–water solution delivered by DME vapor pressure at 4.5 bar. At cathode, air flow rate was 500 ml min^{-1}. Reprinted from [40] with permission from Elsevier.

subsequently reaches saturation. For example, as shown in Fig. 7c, $(CH_3OCH_2-)_{ad}$ reaches the maximum intensity at 0.4 V for ca. 5 s and disappears after ca. 80 s while CO_L increases quickly and reaches saturation after 150 s. It was observed that the formation of CO_L always has a time delay as compared to the formation of $(CH_3OCH_2-)_{ad}$. These two intermediates should be produced in sequence, i.e., $(CH_3OCH_2-)_{ad}$ is formed first and then further decomposed to CO_L. Since the stability of CO_L is much higher than $(CH_3OCH_2-)_{ad}$, once the surface is covered by CO_L, further formation of $(CH_3OCH_2-)_{ad}$ on the same site becomes impossible. In the reviewed work, reliable spectroscopic evidence was

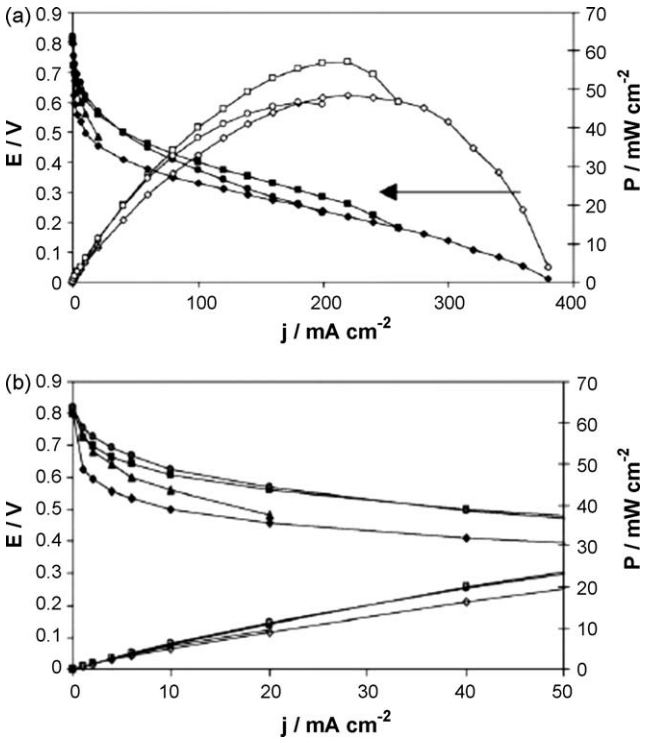

Fig. 12. (a) Cell voltage *E* and power density *P* vs. current density *j* curves in a single 5 cm^2 surface area. Pt/C (◆ and ◇); $Pt_{0.5}Ru_{0.5}$/C (▲ and △); $Pt_{0.8}Ru_{0.2}$/C (■ and □); $Pt_{0.9}Sn_{0.1}$/C (● and ○) anodes at 110 °C (1.65 M DME in water, Nafion® 117 membrane; P_{O_2} = 2 bar; P_{DME} = 3 bar). Reprinted from [42] with permission from Elsevier. (b) Cell voltage *E* and power density *P* for current density j curves for current densities lower than 50 mA cm^{-2} in a single 5 cm^2 surface area FC. Pt/C (◆ and ◇); $Pt_{0.5}Ru_{0.5}$/C (▲ and △); $Pt_{0.8}Ru_{0.2}$/C (■ and □); $Pt_{0.9}Sn_{0.1}$/C (● and ○) anodes at 110 °C (1.65 M DME in water, Nafion® 117 membrane; P_{O_2} = 2 bar; P_{DME} = 3 bar). Reprinted from [42] with permission from Elsevier.

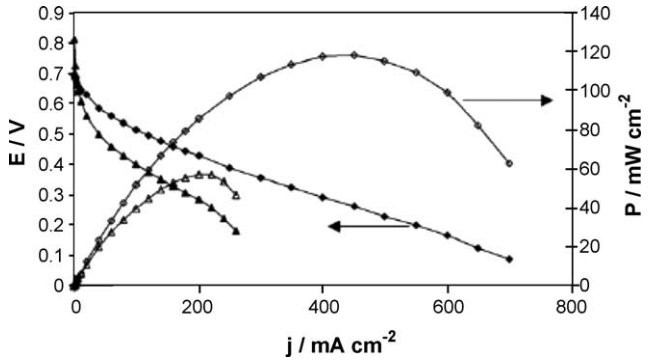

Fig. 13. Cell voltage E and power density P vs. current density j curves in a single 5 cm^2 surface area FC with a $Pt_{0.8}Ru_{0.2}/C$ at 110 °C (Nafion® 117 membrane); (◆ and ◇) MeOH 2.0 M, $P_{O_2} = 3$ bar; $P_{MeOH} = 2$ bar; (▲ and Δ) DME 1.65 M, $P_{O_2} = 2$ bar; $P_{DME} = 3$ bar. Reprinted from [42] with permission from Elsevier.

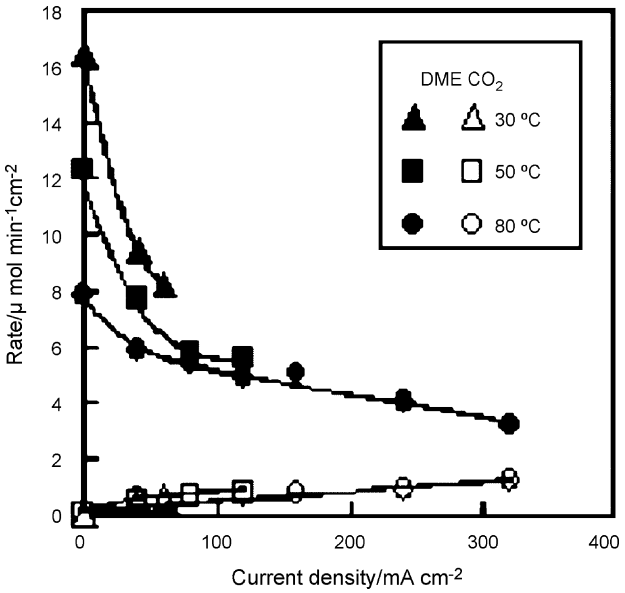

Fig. 14. Dependence of DME and CO_2 exhaust rates in DDMEFC on current density determined by the cathode exhaust. Reprinted from [31] with permission from Elsevier.

obtained to support the C–H cleavage of DME on the Pt electrode surface in relatively low potential regions. Two intermediate reaction species, $(CH_3OCH_2-)_{ad}$ and CO_{ad}, are generated stepwise on the Pt electrode surface during DME decomposition and the electrooxidation process [37]. This conclusion was confirmed by the same authors in [38].

3. Factors affecting on DDMEFCs performance

3.1. Electrocatalysts for DME oxidation

Determining the mechanism of DME oxidation revealed ways to improve the catalytic activity of DDMEFC anode catalysts. As was shown in a previous chapter, one of intermediate products of dimethyl ether oxidation is CO. It is well known that CO is strong poison for platinum materials, which are widely used as a material for fuel cell applications. Significant improvement both in catalytic activity and in stability against the poisonous effect of CO was found in the case of the DMFC anode catalysts based on Pt–M alloys (where M = Ru, Sn, W, Mo) [50–52]. The same principal of using bimetallic platinum-based alloys was used for the determination of the most active catalyst for DME oxidation.

The most comprehensive investigation of Pt–M alloyed catalysts for dimethyl ether oxidation (solution of DME in sulfuric acid) was made by Liu et al. [39]. A number of carbon-supported catalysts with different Pt:M ratios (PtRu/C, Pt_3Sn/C, PtW/C, Pt_3Mo/C, PtCo/C, PtNi/C, Pt_2Cr/C) are compared with a platinum electrocatalyst in Fig. 8. It can be clearly seen that the catalytic activities of PtRu/C and Pt_3Sn/C are significantly higher than Pt/C and other PtM/C catalysts at potentials less than 0.55 V. At $E > 0.6$ V, Pt/C is more active than PtRu/C. This phenomenon can be explained because the poisonous species formed during DME oxidation can be more effectively oxidized to CO_2 on a bare platinum surface at higher over-potentials. As shown in Fig. 9, chronoamperometry provides information on the stability of catalysts against poisonous intermediate species during the DME oxidation. The mass activity as a function of time at 0.4 V decreases drastically within 30 s due to the CO poisoning of all of the catalysts. The stabilized current density of these catalysts at 180 s decreases in the following order: $PtRu/C > Pt_3Sn/C > Pt_3Mo/C > Pt_2Cr/C > PtNi/C > PtCo/C > PtW/C > Pt/C$. PtRu/C demonstrates enhancement by a factor of 12 for the DME oxidation reaction (DOR) over the Pt/C. The factor of Pt_3Sn/C is 4.4, while those of Pt_3Mo/C, Pt_2Cr/C, PtNi/C, PtCo/C, and PtW/C range from 3.4 to 1.3 as compared with Pt/C. The order of performance reflects resistance to CO poisoning and is in good agreement with the activity in Fig. 8. In conclusion, the temperature dependence of DOR for most active catalysts (PtRu/C, Pt_3Sn/C and Pt/C) is shown in Fig. 10 [39]. The apparent activation energy, which was calculated from the slope of the Arrhenius plots, decreases in the following order: PtRu/C (57 kJ mol^{-1}) > Pt_3Sn/C (48 kJ mol^{-1}) ≈ Pt/C (46 kJ mol^{-1}). From above observation, it can be concluded that the addition of a secondary metal enhances the tolerance of Pt to the poisonous species during the DOR. The PtRu/C electrocatalyst shows the most active electrocatalytic activity and the highest tolerance to the poisonous species in the low over-potential range (<0.55 V, 50 °C) amongst the binary electrocatalysts; however, at the higher potential (>ca. 0.55 V, 50 °C), the Pt/C behaves better than PtRu/C.

PtRu is also compared with Pt and Pt/Pd using an MEA evaluation by Yoo et al. as shown in Fig. 11 [40]. Since the Pd black catalyst showed no electrochemical activity for the DME electrooxidation in this study [40], it was tested as a mixed catalyst (50 wt.% of Pt black

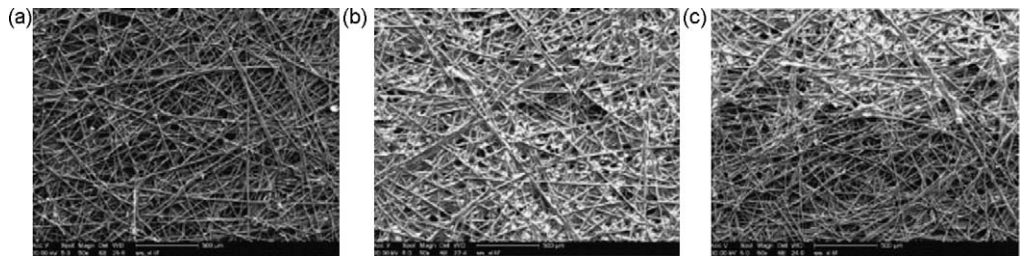

Fig. 15. SEM images of the carbon paper backings of the anodes: (a) E1: hydrophilic anode diffusion layer of MEA; (b) E2: hydrophobic anode diffusion layer of MEA; (c) E3: novel anode diffusion layer of MEA. Reprinted from [44] with permission from Elsevier.

and Pd black). As can be seen in the figure, the PtRu catalyst shows the best performance for the DME electrooxidation, as is similar to the case of methanol electrooxidation. This result is in good agreement with the research of Liu et al. [39].

PtRu/C and PtSn/C with different Pt:Ru ratios were studied by Coutanceau and co-workers [42]. As can be seen from Fig. 12a, the addition of Ru and Sn to platinum does not affect OCV, which remains at about 0.8 V. This effect was explained by Müller et al. [45] with respect to DME crossover. The crossover of DME through Nafion® does not affect the Pt/C cathode catalyst because, at the cathode potential, DME cannot be adsorbed or oxidized on platinum. The constancy of the OCV may indicate that the adsorption of DME by platinum occurs at very close potentials with Ru or Sn, regardless of alloying. Ru and Sn appear to have no ligand effect, the opposite of what happens in the case of methanol adsorption on PtRu alloys [53] and ethanol adsorption on PtSn alloys [54]. On the other hand, the PtRu and PtSn catalysts lead to higher cell voltages in the low current density region than the Pt catalyst does (Fig. 12b). The performance of the fuel cell working with $Pt_{0.5}Ru_{0.5}$, $Pt_{0.8}Ru_{0.2}$ and $Pt_{0.9}Sn_{0.1}$ catalysts is higher than that working with the Pt catalyst up to a current density region of 20, 250 and 180 mA cm^{-2}, respectively. This result can be explained by the bi-functional mechanism in which Ru and Sn are able to activate water molecules at lower potentials to a greater extent than Pt, and thereby bring the missing oxygen atom to complete

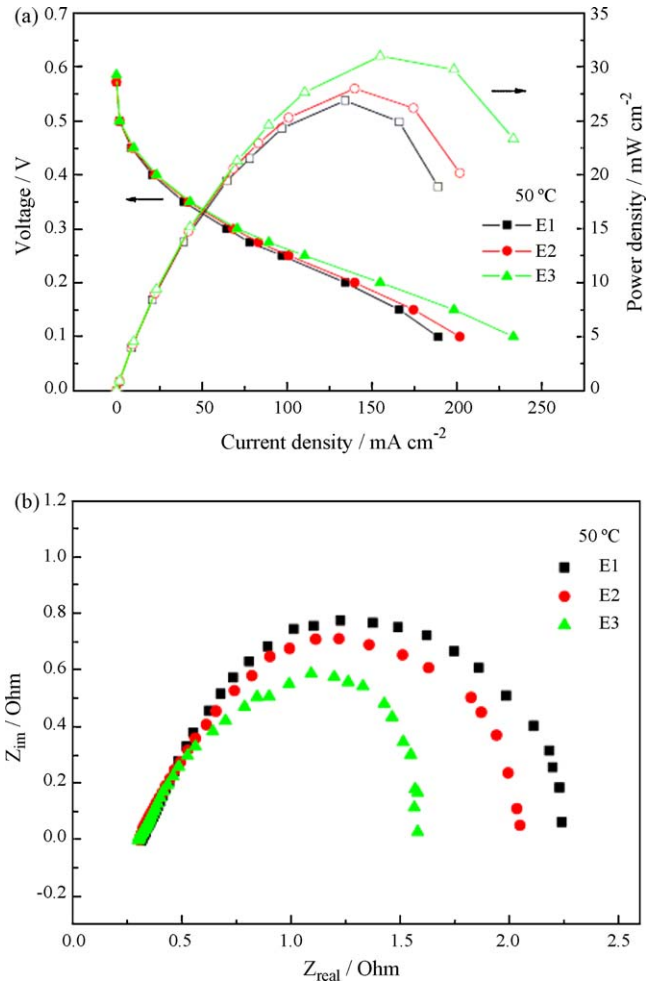

Fig. 16. (a) The polarization curves and the power density curves of MEAs with different anode diffusion layers at 50 °C. Reprinted from [44] with permission from Elsevier. (b) Nyquist diagrams of MEAs with different anode diffusion layers at 400 mV cell voltage and 50 °C. Reprinted from [44] with permission from Elsevier.

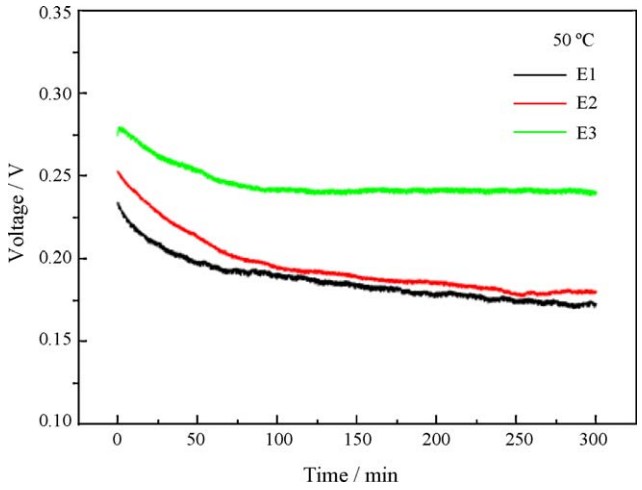

Fig. 17. The constant current operation curves of MEAs with different anode diffusion layers at 100 mA cm^{-2} and 50 °C. Reprinted from [44] with permission from Elsevier.

the oxidation reaction of DME into either CO_2 and/or HCOOH [42]. The $Pt_{0.8}Ru_{0.2}$/C anode appears to be the most active one at 110 °C. However, the presence of ruthenium has an unexpected effect; at high current densities, i.e., below 0.2 V, the voltage decreases rapidly to 0, regardless of the cell temperature, the reactant flow rate, or the pressure. Moreover, this phenomenon is amplified by higher ruthenium content in the catalyst. One possible explanation is that increasing the ruthenium content in the catalyst leads to the dilution of the platinum adsorption sites and a decrease in the accessibility of DME because the adsorption of DME on platinum requires several adjacent sites.

The open question of platinum alloys catalysts containing base metal is durability. In our opinion further experiments using PtSn/C, PtCo/C and PtNi/C are required to determine their behavior under DDMEFC operation conditions.

A comparison of the electrical performances of fuel cells fed with DME solution and methanol was performed by Coutanceau and co-workers [42]. The $E(j)$ and $P(j)$ curves obtained at a cell temperature of 110 °C are given in Fig. 13. Methanol leads to a power density twice as high as DME, i.e., 120 mW cm^{-2} against 60 mW cm^{-2}. Although PtRu is the best catalyst for DME electrooxidation based on the reviewed studies, this catalyst was initially developed and optimized for MeOH oxidation. One of the conclusions of the above research is that the development of new material or the optimization of PtRu for DME oxidation is necessary. The other possibility in increasing of DDMEFC performance is investigation of support effect on the catalytic

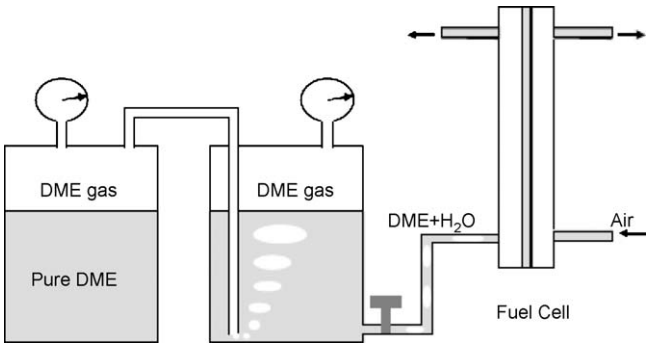

Fig. 18. Schematic view of the experimental test system used in [33]. Reprinted from [33] with permission from Elsevier.

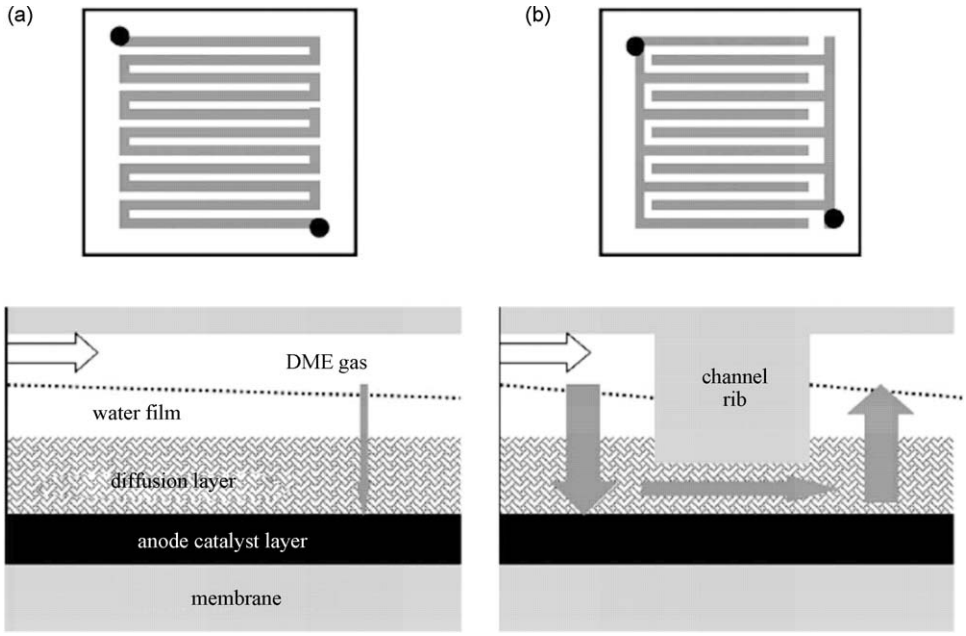

Fig. 19. Schematic diagrams showing the flow of fuels through: (a) serpentine flow field and (b) interdigitated flow field. Reprinted from [33] with permission from Elsevier.

activity of platinum-based materials. For example PtRu/CNT can be candidate for anode catalyst for DME oxidation.

3.2. MEA fabrication and DME crossover

A factor that significantly affected the final fuel cell performance was the MEA fabrication process. Considering the processes taking place on the anode and cathode sides, the fuel supplied to fuel cell, the water management, and so forth, a variety of variables should be tested for optimizing performance, including membrane types, gas diffusion layers (GDLs), and microporous layers (MPLs). Recently, several attempts to estimate the influences of the above parameters were performed [31,35,44].

The influence of the membrane thicknesses on MEA performance was investigated by Mench et al. [35]. Nafion® 117 (thickness is 178 μm) leads to fast drop-off in performance due to the anode over drying. From the other side, thin Nafion® 112 (thickness is 51 μm) cannot be used due to significant crossover of DME or DME intermediates to the cathode side. Nafion® 115 (thickness is 127 μm) promotes the diffusion water from the cathode to the anode side [35].

The DME crossover during MEA operation was studied by Mizutani et al. [31]. To investigate the quantity and explain the characteristics of the fully humidified DME crossover, the gas streams from the cathode and anode were analyzed with GC. MEA was prepared with a Nafion® 112 membrane. The DME and CO_2 exhaust rates are shown in Fig. 14 as a function of current density at 30, 50 and 80 °C. It can be clearly seen from the figure that even at OCV conditions, significant amounts of DME are detected. This result is in agreement with data collected by Mench et al. [35], which suggested that a thin Nafion® 112 membrane can be easy permeated by DME. Fig. 14 shows that DME crossover decreases with increasing the temperature. This is explained by the solubility of DME in water, which decreases with temperature. In addition to this effect, the increase of water vapor pressure with temperature likely decreases the ratio of DME gas in the anode stream. The amount of crossover decreases with an increase in the current density. The DME on the surface of the anode would be consumed more effectively with an increase in the current density, and therefore, the crossover of DME would decrease. Furthermore, the water produced in the cathode also inhibits the gas (DME) permeation, resulting in the reduction of crossover with an increase in the current density. Thus, either a thinner membrane at higher temperature or a thicker membrane at lower temperature should be applied to increase DDMEFC performance.

A detailed investigation of hydrophobic and hydrophilic coatings on the anode GDL surface was made by Cai et al. [44]. The authors compared the performance of MEAs prepared with hydrophobic, hydrophilic and novel diffusion layer types (50% of GDL was coated with hydrophobic PTFE and 50% was coated with hydrophilic Nafion®). A Nafion® 115 membrane was selected for the described investigation. SEM images of the anode carbon paper of MEAs are shown in Fig. 15. Fig. 15a shows that carbon fibers are evenly distributed on the surface of the carbon paper. Fig. 15c shows that the hydrophilic and hydrophobic layers are equally distributed at the surface of the GDL. The combination of these layers should improve water management (hydrophilic layer) as well as DME gas management (hydrophobic layer). The authors used saturated DME solution for the fuel cell tests. Fig. 16a shows the polarization curves and the power density curves of the MEAs

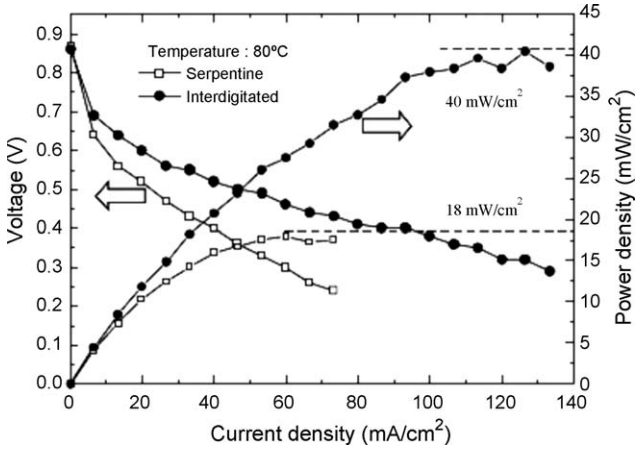

Fig. 20. Effect of flow field pattern on DDMEFC performance at 80 °C. Reprinted from [33] with permission from Elsevier.

with different anode diffusion layers at 50 °C. There is no significant difference in performance for three MEAs operated at a low current density region; however, a new type of MEA (E3) shows the highest activity at a high current density region. Modification of the MEA structure decreases the mass transfer resistance because of improvements in water and DME gas management. To confirm this assumption, electrochemical impedance spectrometry (EIS) was performed to investigate MEAs. Fig. 16b shows that the mass transfer resistance of E3 (novel MEA) is lower than that of E1 (hydrophilic anode diffusion layer of MEA) and E2 (hydrophobic anode diffusion layer of MEA). The novel MEA promotes the mass transport of DME fuel at the anode side. After studying the degradation of MEA performance, a newly designed MEA, which can be used in a new generation of DDMEFCs, is proposed for long term operation (Fig. 17) [44].

3.3. DDMEFCs operation conditions

Optimization of DDMEFC performance by varying conditions such as temperature, flow field types, addition of a second fuel to DME and pressure were studied in the series of works by Cho and co-workers [33,39,40]. A schematic view of their experimental set up is shown in Fig. 18 [33]. The DME reservoir was connected to a water reservoir so as to bubble DME into the water. At room temperature, the saturated DME vapor pressure was 5 bar; both reservoirs were maintained at a pressure of 5 bar during fuel delivery. First, to test the effect of flow field type on DDMFC performance, two flow field types were evaluated: serpentine and interdigitated (Fig. 19). As shown in Fig. 20, MEAs demonstrated lower performance with a serpentine flow field as compared to an interdigitated one. This can be explained by the difference in the mixing of DME and water in the flow field channels. As can be seen from Fig. 19a, in the case of serpentine flow field, the DME–water mixture is separated into two phases, resulting in a lack of contact between the DME and the anode surface. On the other hand, the interdigitated flow field forces the fuel to mix with water during the flow through the diffusion layer at the ribs where the flow channel has been stopped (Fig. 19b). DDMEFC performed poorly at $T = 50$ °C as a result of the high activation energy required for electrooxidation of DME [33].

Later, the same group investigated of pressure influence on DDMEFC performance [40]. The effect of pressure is shown in Fig. 21. Performance was enhanced noticeably with an increase in operating pressure from 1 to 2 bar, while no significant further enhancement was observed at the higher operating pressures of 3–4 bar. In this work, the best performance was 210 mW cm^{-2},

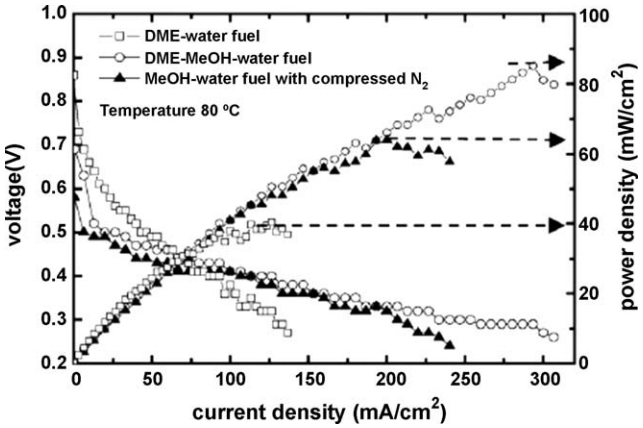

Fig. 21. Effect of pressure in the cells on cell voltage and power density vs. current density curves. Reprinted from [40] with permission from Elsevier.

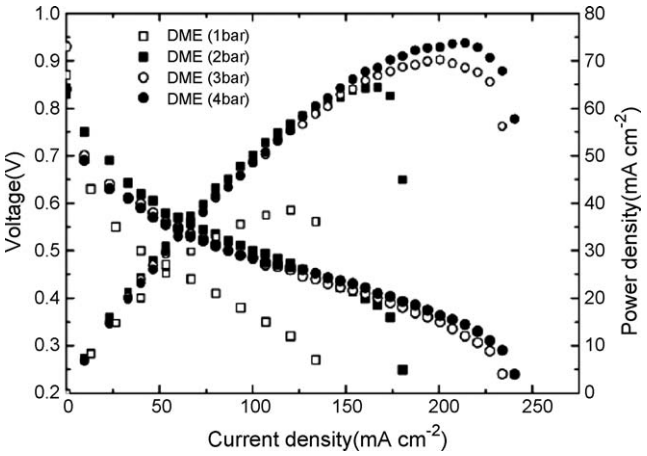

Fig. 22. Effect of methanol mixed with DME–water on the performance of the fuel cell using DME vapor pressure at 4.5 bar. At cathode, air flow rate was 500 ml min^{-1}. Reprinted from [41] with permission from Elsevier.

which was achieved when the fuel cells were operated with the mixed fuel under 4 bar and 80 °C [40].

The third work of Yoo et al., published recently, was devoted to the investigation of DDMEFC by feeding DME with an addition of MeOH [41]. The results of that study are shown in Fig. 22. The authors estimated that methanol was responsible for 76% of the power density, and DME was responsible for the rest. A recommendation for future improvement in DDMEFC performance is that a method must be developed for mixing DME and water for easy delivery to the catalysts; otherwise, the fuel cells should either be operated at temperatures above 100 °C or make use of a mixed fuel as discussed above. This method can be applied to other mixed fuels, such as formic acid and methanol, formic acid and DME, and so forth, for the purpose of enhancing fuel cell performance at low temperatures.

4. Conclusions

In the present review, we tried to summarize recent achievements in development of direct dimethyl ether fuel cells. In contrast with the vast quantity of literature devoted to direct methanol fuel cells, DDMEFC is still a new field for researchers. We have shown that, despite significant attempts to investigate the processes taking place during the DME oxidation, the real mechanism occurring at the anode is still unclear. Uncovering this mechanism should play a major role in the research and development of new effective electrocatalysts for DDMEFCs. At present, only platinum and a limited number of platinum-based catalysts have been investigated, leaving much room for future studies. Some of the catalyst research performed on DMFCs can probably be applied to DDMEFCs. From our point of view, MEA fabrication and operation conditions should be studied in more detail. Taking into account the requirements of conventional battery substitutes for mobile application, we summarize that after improvements in performance, DDMEFC could be a valuable direct liquid fuel cell candidate for commercialization.

References

[1] K. Scott, W. Taama, J. Cruickshank, J. Power Sources 65 (1997) 159–171.
[2] X. Ren, P. Zelenacy, S. Thomas, J. Davey, S. Gottesfeld, J. Power Sources 86 (2000) 111–116.
[3] A. Heinzel, V.M. Barragan, J. Power Sources 84 (1999) 70–74.
[4] V. Baglio, A.S. Aric'o, A. Di Blasi, V. Antonucci, P.L. Antonucci, S. Licoccia, E.S. Fiory, Electrochim. Acta 50 (2005) 1241–1246.
[5] H. Dohle, J. Divisek, J. Mergel, H.F. Oetjen, C. Zingler, D. Stolten, J. Power Sources 105 (2002) 274–282.

[6] X. Ren, T.E. Springer, T.A. Zawodzinski, S. Gottesfeld, J. Electrochem. Soc. 147 (2) (2000) 466–474.
[7] Z. Jusys, T.J. Schmidt, L. Dubau, K. Lasch, L. Jorissen, J. Garche, R.J. Behm, J. Power Sources 105 (2002) 297–304.
[8] Y. Morimoto, E.B. Yeager, J. Electroanal. Chem. 444 (1998) 95–100.
[9] H. William, L.-V.A. Paganin, E.R. Gonalez, Electrochim. Acta 47 (2002) 3715–3722.
[10] Q. Fan, C. Pu, E.S. Smotkin, J. Electrochem. Soc. 143 (1996) 3053–3057.
[11] W.-F. Lin, J.-T. Wang, R.F. Savinell, J. Electrochem. Soc. 144 (1997) 1917–1922.
[12] H. Houa, G. Suna, R. Heb, Z. Wu, B. Sun, J. Power Sources 182 (2008) 95–99.
[13] K. Bergamaski, E.R. Gonzalez, F.C. Nart, Electrochim. Acta 53 (2008) 4396–4406.
[14] E. Ribadeneira, B.A. Hoyos, J. Power Sources 180 (2008) 238–242.
[15] A. Ghumman, P.G. Pickup, J. Power Sources 179 (2008) 280–285.
[16] H. Songa, X. Qiu, D. Guob, F. Li, J. Power Sources 178 (2008) 97–102.
[17] Q. Wang, G.Q. Suna, L. Cao, L.H. Jiang, G.X. Wang, S.L. Wang, S.H. Yang, Q. Xin, J. Power Sources 177 (2008) 142–147.
[18] X. Xue, J. Ge, T. Tian, C. Liu, W. Xing, T. Lua, J. Power Sources 172 (2007) 560–569.
[19] M. Nie, H. Tang, Z. Wei, S.P. Jiang, P.K. Shen, Electrochem. Commun. 9 (2007) 2375–2379.
[20] E. Antolini, J. Power Sources 170 (2007) 1–12.
[21] H. Wang, C. Xu, F. Cheng, S. Jiang, Electrochem. Commun. 9 (2007) 1212–1216.
[22] R. Chetty, K. Scott, Electrochim. Acta 52 (2007) 4073–4081.
[23] L. Zhang, Y. Tang, J. Bao, T. Lua, C. Li, J. Power Sources 162 (2006) 177–179.
[24] S. Wang, N. Kristian, S. Jiang, X. Wanga, Electrochem. Commun. 10 (2008) 961–964.
[25] C. Rice, S. Ha, R.I. Masel, A. Wieckowski, J. Power Sources 115 (2003) 229–235.
[26] W.S. Jung, J. Han, S. Ha, J. Power Sources 173 (2007) 53–59.
[27] X. Wang, Y. Tang, Y. Gao, T. Lua, J. Power Sources 175 (2008) 784–788.
[28] L.J. Zhang, Z.Y. Wang, D.G. Xia, J. Alloys Compds. 426 (2006) 268–271.
[29] K. Brandt, M. Steinhausen, K. Wandelt, J. Electroanal. Chem. 616 (2008) 27–37.
[30] S. Ha, B. Adams, R.I. Masel, J. Power Sources 128 (2004) 119–124.
[31] I. Mizutani, Y. Liu, S. Mitsushima, K. Ota, N. Kamiya, J. Power Sources 156 (2006) 183–189.
[32] G. Kerangueven, C. Coutanceau, E. Sibert, F. Hahn, J.-M. Léger, C. Lamy, J. Appl. Electrochem. 36 (2006) 441–448.
[33] J.-H. Yu, H.-G. Choi, S.M. Cho, Electrochem. Commun. 7 (2005) 1385–1388.
[34] S. Ueda, M. Eguchi, K. Uno, Y. Tsutsumi, N. Ogawa, Solid State Ionics 177 (2006) 2175–2178.
[35] M.M. Mench, H.M. Chance, C.Y. Wang, J. Electrochem. Soc. 151 (2004) A144–A150.
[36] Y. Liu, M. Muraoka, S. Mitsushima, K.-I. Ota, N. Kamiya, Electrochim. Acta 52 (2007) 5781–5788.
[37] Y. Zhang, Le. Lu, Y. Tong, M. Osawa, S. Ye, Electroch. Acta 53 (2008) 6093–6103.
[38] L. Lu, G. Yin, Y. Tong, Y. Zhang, Y. Gao, M. Osawa, S. Ye, J. Electroanal. Chem. 619–620 (2008) 143–151.
[39] Y. Liu, S. Mitsushima, K. Ota, N. Kamiya, Electrochim. Acta 51 (2006) 6503–6509.
[40] J.-H. Yoo, H.-G. Choi, C.-H. Chung, S.M. Cho, J. Power Sources 163 (2006) 103–106.
[41] J.-Y. Im, B.-S. Kim, H.-G. Choi, S.M. Cho, J. Power Sources 179 (2008) 301–304.
[42] G. Kerangueven, C. Coutanceau, E. Sibert, J.-M. Léger, C. Lamy, J. Power Sources 157 (2006) 318–324.
[43] Q. Zhang, Z. Li, S. Wang, W. Xing, R. Yu, X. Yu, Electrochim. Acta 53 (2008) 8298–8304.
[44] K.-D. Cai, G.-P. Yin, J. Zhang, Z.-B. Wang, C.-Y. Du, Y.-Z. Gao, Electrochem. Commun. 10 (2008) 238–241.
[45] J.T. Müller, P.M. Urban, W.F. Hölderich, K.M. Colbow, J. Zhang, D.P. Wilkinson, J. Electrochem. Soc. 147 (2000) 4058–4060.
[46] M. Muraoka, Y. Liu, I. Mizutani, A. Ishihara, S. Mitsuishima, K. Ota, N. Kaniya, J. Hydrogen Energy Syst. Soc. 29 (2004) 51–56.
[47] Y. Tsutsumi, Y. Nakano, S. Kajitani, S. Yamasita, Electrochemistry 70 (2002) 984–987.
[48] S. Wasmus, J.-T. Wang, R.F. Savinell, J. Electrochem. Soc. 142 (1995) 3825–3833.
[49] K. Ota, Y. Nakagawa, M. Takahashi, J. Electrochem. Soc. 179 (1984) 179–186.
[50] A. Damjanovic, M.A. Genshaw, J.O.M. Bockris, J. Electrochem. Soc. 114 (5) (1967) 466.
[51] A.N. Haner, P.N. Ross, J. Phys. Chem. 60 (1975) 267.
[52] J. Wang, H. Nakajima, H. Kita, Electrochim. Acta 35 (1990) 323–328.
[53] P. Waszczuk, A. Wieckowski, P. Zelenay, S. Gottesfeld, C. Coutanceau, J.-M. Léger, C. Lamy, J. Electroanal. Chem. 511 (2001) 55–64.
[54] F. Vigier, C. Coutanceau, F. Hahn, E.M. Belgsir, C. Lamy, J. Electroanal. Chem. 563 (2004) 81–89.